Predatory selection of mucoid, antibiotic resistant *Pseudomonas putida* phenotype by myxobacterium *Cystobacter ferrugineus*

Shukria Akbar[a] and D. Cole Stevens[a,#]

Department of BioMolecular Sciences, University of Mississippi, University, MS, USA[a]

Running Head: Predatory selection of antibiotic resistant *P. putida*

#Address correspondence to D. Cole Stevens, stevens@olemiss.edu.

Abstract: Predation contributes to the structure and diversity of microbial communities. Predatory myxobacteria are ubiquitous to a variety of microbial habitats and capably consume a broad diversity of microbial prey. Predator-prey experiments utilizing myxobacteria have provided details into predatory mechanisms and features that facilitate consumption of prey. However, prey resistance to myxobacterial predation remains underexplored, and prey resistances have been observed exclusively from predator-prey experiments that included the model myxobacterium *Myxococcus xanthus*. Utilizing a predator-prey pairing that instead included the myxobacterium, *Cystobacter ferrugineus,* with *Pseudomonas putida* as prey, we infrequently observed surviving phenotypes capable of eluding predation. Comparative transcriptomics between *P. putida* unexposed to *C. ferrugineus* and the survivor phenotype suggested that increased expression of efflux pumps, genes associated with mucoid conversion, and various membrane features contribute to predator avoidance. The *P. putida* survivor phenotype was confirmed to be resistant to the antibiotics kanamycin, gentamicin, and tetracycline and to produce more alginate, pyoveridine, and phenazine-1-carboxylic acid than predator-unexposed *P. putida*. Unique features observed from the survivor phenotype including small colony variation, efflux-mediated antibiotic resistance, phenazine-1-carboxylic acid production, and increased mucoid conversion overlap with traits associated with *Pseudomonas aeruginosa* predator avoidance and pathogenicity. The survivor phenotype also benefited from increased predator resistance during subsequent predation assays. These results demonstrate the utility of myxobacterial predator-prey models and provide insight into prey resistances in response to predatory stress might contribute to the phenotypic diversity and structure of bacterial communities.

35 **Introduction**

36 Abundant within soils and marine environments, predatory myxobacteria contribute to
37 nutrient cycling within the microbial food web (1-4). Myxobacteria are prolific producers
38 of antimicrobial specialized metabolites and display a cooperative, swarming predation
39 strategy that can be readily reproduced and monitored within laboratory settings making
40 them uniquely appropriate for assessment of predator-prey interactions (1, 3-5). Broadly
41 considered generalist predators, myxobacteria capably predate a range of prey including
42 both Gram-negative and Gram-positive bacteria as well as fungi (5, 6). Constitutive
43 production of specialized metabolites and lytic proteins are often associated with this
44 predatory range, and a variety of metabolites and enzymatic features have been reported
45 to benefit predation (7-10).

46 However, relatively few examples of prey resistance to myxobacterial predation have
47 been reported (11). Compared to features associated with bacterial strategies to avoid
48 protozoan predators, prey avoidance of predatory myxobacteria remains underexplored
49 (12-16). Examples of prey responses correlated with resistance to myxobacterial
50 predation include *Escherichia coli* biofilm formation (17), *Bacillus subtilis* sporulation and
51 production of bacillaene (18, 19), *Bacillus licheniformus* glycosylation of the predation-
52 associated metabolite myxovirescin A (20), galactoglucan exopolysaccharide production
53 and increased melanin production by *Sinorhizobium meliloti* (21, 22), and formaldehyde
54 secretion by *Pseudomonas aeruginosa* (11). All of these features were discovered from
55 predator-prey experiments utilizing the model myxobacterium *M. xanthus*.

56 We suspect the development of predator-prey pairings including myxobacteria other than
57 *M. xanthus* might provide additional insight into prey resistance to myxobacterial

58 predation. For our predator-prey experiments, the soil dwelling myxobacterium
59 *Cystobacter ferrugineus* strain Cbfe23 was included due to a favorable growth profile and
60 capability to quickly consume *P. putida* during standard predation assays (23-25). Also
61 found within soils, root colonizing *P. putida* was chosen as prey due to an established
62 ability to resist protozoan grazers (14). Initial predator-prey experiments provided a *P.*
63 *putida* phenotype capable of avoiding *C. ferrugineus* predation. Herein we report the
64 generation and predator avoidance of a *P. putida* phenotype resistant to myxobacterial
65 predation using standard predator-prey experiments, differential gene expression data
66 comparing the survivor phenotype with predator-unexposed *P. putida*, and traits observed
67 to potentially contribute to predator avoidance.

68 **Results**

69 **Selection of predation resistant *P. putida* phenotype**

70 Utilizing predation assays where an inoculum of *C. ferrugineus* was introduced to the
71 edge of an established spot of *P. putida* (24), we considered swarming overtaking the *P.*
72 *putida* spot with no visible prey remaining to be an endpoint for assessment of remaining
73 viable prey cells using colony forming unit (CFU) assays. Typically, *C. ferrugineus*
74 swarmed predation sensitive *P. putida* with no visible prey after 3 days of co-cultivation
75 on nutrient restrictive WAT agar (Figure 1A and 1D). However, from 100 total assays 5
76 provided minimally consumed and readily observable *P. putida* remaining after 10-14
77 days (Figure 1B and 1D). Additionally, instead of frontal attack at the predator-prey
78 interface when exposed to predation sensitive *P. putida*, *C. ferrugineus* swarmed the
79 perimeter of the survivor phenotype (Supplemental Figure 1). Exponentially fewer viable
80 colonies of predation sensitive *P. putida* were observed from endpoint CFU assays (3-4

81 days for predation sensitive *P. putida*; 10-14 days for *P. putida* survivor phenotype)
82 supporting the assumption that swarming resistance correlates with prey survival (Figure
83 1D and 1E). Also apparent from CFU assays, colonies of the survivor phenotype were
84 consistently smaller when compared to predation sensitive *P. putida* (Figure 1C).
85 Predation resistance of the survivor phenotype was also observed from additional
86 predation assays with the optical density of prey inoculum doubled (OD_{600}=1.0 versus
87 OD_{600}=0.5). (Supplemental Figure 2). Stocks of each *P. putida* survivor observed from
88 predation assays were stored at -80°C as individual aliquots and utilized to determine
89 features associated with the survivor phenotype that might contribute to predator
90 avoidance.

91 **Differential gene expression of predator-unexposed *P. putida* and survivor**
92 **phenotype**

93 Utilizing RNA sequencing, we conducted comparative transcriptomic experiments
94 between the predator unexposed (control) *P. putida* and the survivor phenotype (n=3
95 biological replicates with biological replicates for the survivor phenotype defined as an
96 individually observed phenotype resistant to *C. ferrugineus* predation for ≥10 days). This
97 comparative analysis determined that 1,178 genes were down-regulated ≥4-fold and 122
98 genes were up-regulated ≥4-fold across the survivor phenotype replicates when
99 compared to control *P. putida* replicates (n=3; $p \leq 0.05$). Considering up-regulated genes
100 from the survivor phenotype with the highest fold change values, apparent differences in
101 overexpressed features specific to the survivor phenotype included genes involved in
102 mucoid conversion, siderophore production, and a variety of membrane-associated
103 proteins (Figure 2A). A 4 gene operon including a ferric uptake regulatory (*furA*)

104 associated gene (WP_016501343.1), a fumarate hydratase (WP_016501342.1), a
105 manganese superoxide dismutase (*sodA*) (WP_016501340.1), and a hypothetical protein
106 with a conserved DUF2753 domain (WP_06501341.1) was significantly up-regulated in
107 the survivor phenotype (Figure 2B and 2C). Expression of this operon from *P. aeruginosa*
108 in response to iron limitation leads to elevated alginate production, an exopolysaccharide
109 composed of mannuronic acid and guluronic acid monomers, and increased mucoidy (26,
110 27) and corroborates our observation of small colony variance from the survivor
111 phenotype. Interestingly, the alginate regulatory elements MucA (WP_016498171.1) and
112 MucB (WP_016498172.1) were both significantly down regulated in the survivor
113 phenotype (Figure 2B). The anti-sigma factor MucA and the associated binding partner
114 MucB inhibit mucoid conversion by sequestering the alternative sigma factor AlgU
115 required for alginate production in *P. aeruginosa* (28-31). Increased transcription from the
116 4 gene, *furA* operon combined with decreased transcription of MucA and MucB, indicates
117 that mucoid conversion might contribute to predator avoidance which parallels *P.*
118 *aeruginosa* predatory avoidance mechanisms when exposed to grazing amoeba (32).

119 Also associated with iron limitation, regulatory and biosynthetic genes contributing to
120 production of the siderophore pyoverdine were significantly up-regulated in the survivor
121 phenotype. These included PvdA an L-ornithine monooxygenase (WP_016499102.1)
122 and PvdH a diaminobutyrate-2-oxoketoglutarate transaminase (WP_016498669.1) both
123 involved in pyoverdine precursor biosynthesis, a regulatory transcription factor PvdS
124 (WP_016498655.1), a proximal MbtH-like protein (WP_016499090.1), and a core
125 nonribosomal peptide synthetase homologous to PvdL from *P. aeruginosa*
126 (NP_746359.1) (Supplemental Figure 3) (33-36). Also associated with iron limiting

127 conditions, a bacterioferritin-associated ferredoxin (WP_016488781.1) was upregulated
128 in the survivor phenotype.

129 A variety of membrane-associated proteins were also overexpressed in the survivor
130 phenotype including an osmotically inducible protein OsmY (WP_0016501632.1), an
131 outer membrane protein A (OmpA) family protein (WP_016501196.1), an FKBP-type
132 peptidyl-prolyl cis-trans isomerase (WP_0165010671), an aquaporin (WP_016498616.1),
133 and a DUF1282 domain-containing hypothetical protein from the Yip1 superfamily
134 (WP_016499858.1) (Figure 2A). While not a membrane associated feature, we also found
135 the overexpression of a formaldehyde dehydrogenase (WP_016497631.1) by the
136 survivor phenotype to be of note due to the recent observation that suggests
137 formaldehyde secretion to be a predation-resistance trait of *P. aeruginosa* (11). The
138 abundance of up-regulated genes that encode membrane-associated products in the
139 survivor phenotype including those responsible for increased mucoid production provides
140 insight into features involved in predation avoidance.

141 Numerous efflux and transport proteins were also among the most up-regulated genes
142 observed from the survivor phenotype (Figure 2D). Upregulated efflux genes included
143 inner (WP_016498130 and WP_016499477.1) and outer (WP_016498128.1) membrane
144 components highly homologous to the AcrAD-TolC-type multidrug resistance-nodulation-
145 division (RND) family of efflux pumps and the Mex RND efflux pumps known to facilitate
146 *P. aeruginosa* resistance to aminoglycosides and tetracyclines (37-39). Genes encoding
147 features homologous to multidrug efflux pumps contributing to virulence of human
148 pathogens were also up-regulated in the survivor phenotype including a P-type ATPase
149 (WP_016502100) and an additional RND/MmpL (Mycobacterial membrane protein

150 Large) protein (Figure 2D). Afforded these observed differences in gene expression, we
151 sought to determine if the survivor phenotype demonstrated antibiotic resistance,
152 increased mucoidy, and increased production of the siderophore pyoverdine which have
153 all been previously associated with predator avoidance strategies.

154 **Antibiotic resistance of survivor phenotype**

155 Provided the observation that numerous transport proteins were overexpressed in the
156 survivor phenotype (Figure 2D) including RND-type efflux pumps known to contribute to
157 *P. aeruginosa* antibiotic resistances, we were interested to determine if the survivor
158 phenotype exhibited antibiotic resistance. The survivor phenotype was capable of initially
159 forming colonies on LB agar supplemented with the antibiotics gentamicin (10 μg/ml),
160 kanamycin (50 μg/ml), and tetracycline (10 μg/ml), with no colonies from predation
161 sensitive *P. putida* observed on identical medias. Subsequent growth curve assays
162 comparing predation sensitive *P. putida* with the survivor phenotype when grown in LB
163 and LB supplemented with antibiotics (Figure 3A and 3B) confirmed that the survivor
164 phenotype was uniquely resistant to gentamicin, kanamycin, and tetracycline. These
165 results combined with the overexpression of efflux-associated proteins observed from the
166 survivor phenotype confirms that *C. ferrugineus* selection provides prey that benefit from
167 antibiotic resistance and suggests efflux-mediated antibiotic resistance to be involved in
168 *P. putida* response to predatory stress.

169 **Increased production of alginate by survivor phenotype**

170 Alginate-based formation of mucoid biofilms has previously been associated with *P.*
171 *aeruginosa* avoidance of the protozoan grazer *Rhynchomonas nasuta* (32, 40-42).
172 Utilizing an established carbazole assay as well as alginate antibody dot blots (43-45),

173 we sought to determine if the increased transcription of genes known to impact alginate
174 production observed from the survivor phenotype resulted in increased production of
175 alginate when compared to predator unexposed *P. putida*. Comparing supernatants from
176 predation sensitive *P. putida* with the survivor phenotype, we observed that the survivor
177 phenotype indeed produced more alginate when compared to *P. putida* not exposed to
178 *C. ferrugineus* (Figure 4).

179 **Increased pyoverdine production by survivor phenotype**

180 Significantly upregulated features associated with pyoverdine biosynthesis previously
181 noted from the survivor phenotype in our transcriptomic data suggested that increased
182 pyoverdine production might be an observable survivor trait. Fluorescence of extracellular
183 pyoverdine was quantified from clarified medias of predator unexposed *P. putida* and the
184 survivor phenotype using methodology established by Imperi *et al* (46, 47). Indicative of
185 increased pyoverdine secretion, extracellular fractions from the survivor phenotype
186 exhibited a 3-5 fold increase in fluorescence when compared to extracellular fractions
187 from predator unexposed *P. putida* (Figure 5). Although the genome of the *P. putida* type
188 strain includes a pyoverdine biosynthetic gene cluster, no structurally elucidated
189 pyoverdines have been characterized from the *P. putida* type strain, and these results
190 merely suggest the presence of fluorescent pyoverdine-like metabolites potentially
191 produced by the strain. Regardless, these results corroborate overexpression of
192 pyoverdine biosynthetic pathway components observed in our transcriptomic analysis
193 and suggest that pyoverdine production may contribute to the predator avoidance trait of
194 the survivor phenotype.

195 **Increased production of phenazine-1-carboxylic acid by survivor phenotype**

196 Untargeted mass spectrometry was used to assess additional differences in detectable
197 quantities of *P. putida* metabolites comparing organic phase extracts from predator
198 unexposed *P. putida* and the survivor phenotype. Initial analysis of resulting data using
199 Global Natural Product Social Molecular Networking (GNPS) (48) resulted in a library hit
200 for phenazine-1-carboxylic acid ([M+H]=225.066) that was only observed in extracts from
201 the survivor phenotype (Figure 6A). Subsequent comparison utilizing XCMS-MRM (49)
202 provided the statistical significance (n=3; p=0.0509) in detected phenazine-1-carboxylic
203 acid between extracts from predator unexposed *P. putida* and the survivor phenotype
204 (Figure 6B). Interestingly, phenazine production in *P. aeruginosa* contributes to redox
205 maintenance during biofilm formation and promotes efflux-based antibiotic resistance
206 (50-53). Despite no significant change in expression of putative phenazine biosynthesis
207 genes *phzD* (SUD74861.1) and *phzF* (SUD71919.1) from our comparative transcriptomic
208 data (54-57), we suspect that higher quantities of phenazine-1-carboxylic acid detected
209 in extracts from the survivor phenotype may contribute to the increased transcription of
210 efflux pump components and antibiotic resistance observed from the survivor phenotype.
211 However, associations between phenazine production and efflux-mediated resistance
212 have only been reported from *P. aeruginosa*, and any parallels potentially observed in our
213 data require further investigation. Also of note, phenazine production has been observed
214 to protect *Pseudomonas aureofaciens* from predatory myxobacteria (58). These results
215 suggest that the survivor phenotype produces significantly greater quantities of
216 phenazine-1-carboxylic acid when compared to predator-unexposed *P. putida*.

217 **Predation resistance of survivor phenotype in subsequent predation assays**

218 Additional subsequent predation assays were done to assess the predator avoidance trait
219 of the *P. putida* survivor phenotype with *P. putida* not exposed to *C. ferrugineus* included
220 as a control. These predation assays included an assay as previously described with
221 predator cells directly introduced to the edge of established prey, a similar slightly
222 modified assay with predator introduced at a distance of 5-7 mm from an established spot
223 of *P. putida*, and a lawn culture assay (23) monitoring predator swarming diameters when
224 placed at the center of prey embedded in agar. For direct contact assays, time to complete
225 swarming was recorded. As observed in our prior predator-prey experiments, compared
226 to control *P. putida* the survivor demonstrated significantly increased predator avoidance
227 (Figure 7A). The survivor phenotype also demonstrated resistance to swarming
228 compared to predation sensitive *P. putida* during identical direct-contact predation assays
229 conducted on nutrient-rich VY/2 agar (Supplemental Figure 4) For indirect contact
230 predation assays, time to predator-prey contact and time to complete swarming were
231 recorded. Time to predator-prey contact was between 1-2 days for all samples, and as
232 observed in the directed contact predation assays the survivor phenotype demonstrated
233 increased predator avoidance when compared to control *P. putida* (Figure 7B and 7C).
234 However, no differences between swarming diameters of *C. ferrugineus* grown on lawns
235 of control *P. putida* and the *P. putida* survivor phenotype were observed (Figure 7D).
236 These data suggest the *P. putida* survivor phenotype benefits from a predator avoidance
237 trait when subjected to 2 out of 3 subsequent predation assays.

238 **Discussion**

239 Building upon previously reported resistance strategies to avoid predatory myxobacteria
240 discovered from predator-prey experiments (11, 17-22), predation experiments including

241 *C. ferrugineus* and *P. putida* provided a prey phenotype significantly resistant to
242 predation. Traits associated with prey resiliency during bacterial predator-prey
243 interactions remain underexplored despite growing evidence that predatory stress
244 contributes to the development of phenotypic traits associated with persistent clinical
245 pathogens (12, 16, 59). As an example, clinical isolates of persistent *P. aeruginosa* from
246 cystic fibrosis patients exhibit increased mucoidy and small colony variation as well as
247 efflux-mediated antibiotic resistance (60-62). Other human pathogens that have
248 demonstrated overlapping factors involved in both virulence and anti-predation strategies
249 include *Legionella pneumophila*, *Escherichia coli*, *Vibrio cholerae*, *Campylobacter jejuni*,
250 *Listeria monocytogenes*, *Mycobacterium leprae*, and *Yersinia enterocolitica* (12, 16).
251 Overlapping factors thus far observed to be associated with both virulence and predator
252 avoidance include biofilm formation (15, 32, 42), quorum signal (63) and siderophore (64)
253 small molecule biosynthesis, toxin production (65-67), expression of transport proteins
254 such as type III and type VI secretion systems (68, 69) and antibiotic resistance-
255 associated efflux pumps (70, 71). While the impact of predatory selection on virulence
256 factors have primarily been reported from predator-prey experiments with grazing
257 amoeba, efforts to determine the influence of generalist predators on microbial
258 communities have suggested that bacterial predators also drive adaptation of prey traits
259 that overlap with virulence in bacterial pathogens (5). Recently, Nair *et al.* reported that
260 during predator-prey interactions with *E. coli* prey, the predatory myxobacterium
261 *Myxococcus xanthus* selects for 2 traits associated with virulence, mucoidy and increased
262 expression of the outer membrane protease OmpT (5). Compared to features associated
263 with bacterial strategies to avoid protozoan predators, prey avoidance of myxobacterial

264 predators remains underexplored. Although predator-prey experiments that utilize
265 myxobacteria with various prey such as *Bacillus subtilis* (9, 18, 19), *E. coli* (5, 7),
266 *Sinorhizobium melilotti* (21, 22), *P. aeruginosa* (11), and *Streptomyces coelicolor* (72)
267 have been reported, all myxobacterial resistances have been discovered from predator-
268 prey experiments that included the model myxobacterium *M. xanthus*. Utilizing an
269 alternative myxobacterium *C. ferrugineus* provides the opportunity to further compare
270 predatory selection and adaptive prey avoidance strategies.
271 Comparative transcriptomics provided key features up-regulated in the *P. putida* survivor
272 phenotype that overlap with traits associated with *P. aeruginosa* predator avoidance and
273 pathogenicity. Of these, 3 putative RND family transporter components with high
274 homology to the MexAB-OprM and MexCD-OprM efflux systems known to mediate *P.*
275 *aeruginosa* antibiotic resistance were up-regulated in the survivor phenotype (38, 39).
276 Growth curve analysis determined that the *P. putida* survivor phenotype was indeed
277 resistant to the aminoglycosides kanamycin and gentamicin as well as tetracycline;
278 susceptibility to all 3 of these antibiotics was observed from predator unexposed *P. putida*.
279 Also of note, the multidrug efflux pump CmeABC serves as a survival mechanism for *C.*
280 *jejuni* when engulfed by the predatory amoeba *Acanthamoeba polyphaga* (71).
281 Several features associated with mucoid conversion were also up-regulated in the
282 survivor phenotype including a 4 gene operon responsible for elevated alginate
283 production in *P. aeruginosa* and the regulatory transcription factors MucA and MucB (26-
284 28, 30). Adaptive mucoid phenotypes have been previously observed in response to
285 myxobacterial predation (5), amoebal grazing (40), macrophages (73), and lytic phages
286 (74). Increased alginate production by the survivor phenotype was confirmed using

287 established carbazole assays and anti-alginate dot blots. Alginate-based mucoid
288 conversion and biofilm formation have previously been associated with *P. aeruginosa*
289 avoidance of grazing amoeba and could also contribute to the small colony variation
290 observed from our survivor phenotype (32, 40, 41). These results and the observed
291 alternative predatory pattern of *C. ferrugineus* during predator-prey interactions with the
292 survivor phenotype parallel previous observation of mucoid *S. meliloti* phenotypes
293 avoiding *M. xanthus* predation (22). Additionally, upregulation of an OmpA family protein
294 observed in the survivor phenotype might also correlate with mucoid conversion as *P.*
295 *aeruginosa* phenotypes that upregulate expression of OmpA also overproduce alginate
296 (75). These results provide clear overlap between features contributing to avoidance of
297 myxobacterial and amoebal predation and also afford additional evidence that the
298 coincidental selection of prey virulence factors reported from amoebal predatory stress
299 (12) might also be observed from predator-prey interactions involving myxobacteria. Both
300 efflux-mediated antibiotic resistance and mucoid conversion have also been attributed to
301 virulence of clinical isolates of *P. aeruginosa* (29, 59, 60, 76).
302 Additionally, our data provided key areas for follow-up investigations to assess the
303 chemical ecology of the predator-prey interface and its contribution to predator avoidance
304 such as the increased production of pyoverdines and phenazine-1-carboxylic acid
305 detected from the survivor phenotype. For example, up-regulation of the pyoverdine
306 biosynthetic pathway and a bacterioferritin-associated ferredoxin as well as increased
307 pyoverdine in extracellular extracts observed from the survivor phenotype suggests an
308 iron-depleted predator-prey environment similar to the previously reported interaction
309 between *M. xanthus* and *Streptomyces coelicolor* (72). Enhanced production of the

310 primary myxobacterial siderophore myxochelin by *M. xanthus* contributed to an iron-
311 restrictive environment and triggered production of the pigment actinorhodin from *S.*
312 *coelicolor.* Further investigation focused on the chemical ecology of predator-prey
313 interfaces might also shed light on the various membrane features observed to be up-
314 regulated in the survivor phenotype.
315 The survivor phenotype was also assessed with subsequent predation assays to
316 determine the resiliency of the predator avoidance trait. While comparative transcriptomic
317 data provided insight into key up-regulated features potentially involved in prey survival,
318 down-regulation of 1,178 genes in the survivor phenotype when compared to predator
319 unexposed *P. putida* suggests potentially diminished survivor fitness. Despite this, the
320 survivor phenotype maintained the predator avoidance trait in 2 out of 3 subsequent
321 predation assays. While it is unclear why no significant predator avoidance was observed
322 from lawn culture predation assays, we suspect the introduction of predator to the center
323 of prey lawns as opposed to consistent introduction to the peripheral interface of prey
324 potentially reduce any predator avoidance mechanisms. Predator avoidance observed
325 from direct and indirect contact predation assays and the heterogeneity associated with
326 differences between the growth and metabolism of peripheral cells and central cells of
327 bacterial colonies supports this suspicion (77, 78). Perhaps belaboring, we also suggest
328 that these results again highlight the importance of chemical exchange at the predator-
329 prey interface. We anticipate that *P. putida* phenotypes resistant to myxobacterial
330 predation continually subjected to such predatory selection will afford adapted
331 phenotypes for further scrutiny of any resulting mutations and genotypes. Ultimately,
332 these results demonstrate the utility of predator-prey experiments using lesser studied

333 myxobacteria and provide insight into how predatory stress might contribute to adaptive
334 phenotypic diversity of bacterial communities.

335 **Materials and Methods**

336 **Bacterial Strains and Cultivation**

337 The myxobacterium *Cystobacter ferrugineus* strain Cbfe23, DSM 52764 was employed
338 as the predator. *Pseudomonas putida* type strain, ATCC 12633, and the discussed *P.*
339 *putida* survivor phenotype resulted from predation assays with this *P. putida* type strain
340 were included as prey. *C. ferrugineus* was grown on VY/2 solid (1.4% w/v agar, 0.1% w/v
341 $CaCl_2$ * 2 H_2O, 0.5% w/v Baker's yeast, 500 µM vitamin B12) media for 5-7 days. Luria-
342 Bertani (LB) solid (1.5% agar) and liquid media were utilized for the cultivation of *P.*
343 *putida*. Predation experiments were performed on WAT agar (1.5% w/v agar, 0.1% w/v
344 $CaCl_2$, 20 mM HEPES) plates. All bacteria were grown at 30 °C.

345 **Predation assays**

346 Prey spot assay was performed as described by Seccareccia et al. (24). Briefly, *P. putida*
347 prey was grown in LB liquid media on a rotary shaker (150 rpm) at 30 °C for 16-18 h.
348 Next, the bacterial cultures were sedimented by centrifugation at 4,000 g for 15 min, and
349 the sedimented cells were washed and resuspended in TM buffer (50 mM Tris, pH 7.8,
350 10 mM $MgSO_4$) to an OD_{600} of 0.5. Then the WAT agar plates were spotted with 150 µl
351 of the freshly prepared bacterial suspensions, and the spots were dried in a laminar flow
352 hood. Finally, *C. ferrugineus* was inoculated at the edge of the prey spot. The assay plates
353 were incubated at 30 °C for 14 days or until the full visible swarming of *C. ferrugineus* on
354 the prey spot. The assay was performed with 100 replicates. Any prey spot with visible
355 biomass of *P. putida* after day 14 was considered as survivor phenotype of *P. putida*, and

356 five observed *P. putida* survivor stocks were acquired that remained visible after day 14
357 of the assay.
358 For subsequent predation assays, *P. putida* predation sensitive (control) and the survivor
359 phenotypes were employed as prey. The direct spot assay was performed as mentioned
360 above. Statistical significance of recorded time to predation reported in was calculated
361 using an unpaired t test with Welch's correction in Prism 7.0d. The subsequent directed
362 contact predation assay was performed on VY/2 (1.4% w/v agar, 0.1% w/v $CaCl_2$ * 2 H_2O,
363 0.5% w/v Baker's yeast, 500 μM vitamin B12) media as well, considered as nutrient-rich
364 media. For indirect contact spot assay, *C. ferrugineus* was inoculated at a distance of 5-
365 7 mm from the established *P. putida* control and *P. putida* survivor prey spots. Next, time
366 *C. ferrugineus* took to reach the prey spots and the time of its swarming over the spots
367 was recorded. Indirect predation assays were performed with 8 replicates per phenotype.
368 Statistical significance of recorded time to predation reported in days and recorded time
369 to initial contact between *C. ferrugineus* and prey reported in days was calculated using
370 an unpaired t test with Welch's correction in Prism 7.0d.
371 Swarming predation assays were based on established lawn culture methods (23). In
372 brief, *P. putida* prey phenotypes were grown in LB liquid media for 16-18 h at 30 °C with
373 shaking at 150 rpm. The cultures were then subjected to centrifugation at 4,000 g for 15
374 min, and the sedimented cells were washed and resuspended in TM buffer (50 mM Tris,
375 pH 7.8, 10 mM $MgSO_4$) to an OD_{600} 0.5. Next, 1 ml of the cell suspension was spread
376 onto a 14 cm diameter WAT agar plate and dried to form a uniform prey lawn. Finally, *C.*
377 *ferrugineus* previously cultured on VY/2 agar media was spotted onto the center of the
378 prey lawn. The assay plates were incubated at 30 °C, and the expansion of the *C.*

379 *ferrugineus* swarm was measured on day 4. Lawn culture predation assays were
380 performed with 8 replicates per phenotype with replicates from each survivor stock
381 included. All 3 predation assays were performed simultaneously for all replicates.
382 Statistical significance of *C. ferrugineus* swarm diameters reported in millimeters on day
383 4 was calculated using an unpaired t test with Welch's correction in Prism 7.0d

384 **CFU assays.**

385 The colony forming units (CFU) were calculated as described by DePas *et al.* (17). Briefly,
386 after the full swarming of *C. ferrugineus* over the prey spot, the agar slab under the prey
387 spot was excised and suspended in 2 mL phosphate buffer saline (PBS). Next, a dilution
388 series from this solution was inoculated on the LB plates, and the plates were incubated
389 at 30 °C for 18 hr. Then, CFU/mL was calculated from the viable colonies that appeared
390 on the LB plates. Finally, the CFU/mL of the survivor was compared with CFU/mL of the
391 unexposed *P. putida,* considered as a control. Statistical significance of all CFU assays
392 was calculated using an unpaired t test with Welch's correction in Prism 7.0d.

393 **RNA sequencing**

394 Triplicate samples of *P. putida* control and *P. putida* survivor phenotype grown from
395 stocks in LB at 37°C for 18 hr and pelleted via centrifugation were stored in RNA*later*
396 solution for sequencing. The DNA from *P. putida* type strain cells (200 μl) was extracted
397 using MagAttract HMW DNA Kit (Qiagen). The DNA was eluted in 100 uL AE buffer. The
398 concentration of DNA was evaluated (Supplementary Table 1) using the Qubit® dsDNA
399 HS Assay Kit (Life Technologies). The library was prepared using Nextera DNA Flex
400 library preparation kit (Illumina) following the manufacturer's user guide. 50 ng DNA was
401 used to prepare the library. The sample underwent the simultaneous fragmentation and

402 addition of adapter sequences. These adapters are utilized during a limited-cycle (6
403 cycles) PCR in which unique index was added to the sample. Following the library
404 preparation, the final concentration of the library (Supplementary Table 1) was measured
405 using the Qubit® dsDNA HS Assay Kit (Life Technologies), and the average library size
406 (Supplementary Table 1) was determined using the Agilent 2100 Bioanalyzer (Agilent
407 Technologies). The library was diluted (to 6.5 pM) and sequenced paired end for 500
408 cycles using the MiSeq system (Illumina).
409 Total RNA was isolated from triplicate samples of the *P. putida* control, the *P. putida*
410 survivor phenotype from stocks, and the kanamycin resistant phenotype using the
411 RNeasy PowerSoil Total RNA Kit (Qiagen) following the manufacturer's instructions. 400
412 μl cell sample was used for extractions. The concentration of total RNA was determined
413 (Supplementary Table 2) using the Qubit® RNA Assay Kit (Life Technologies). For rRNA
414 depletion, first, 1000 ng of total RNA was used to remove the DNA contamination using
415 Baseline-ZERO™ DNase (Epicentre) following the manufacturer's instructions followed
416 by purification using the RNA Clean & Concentrator-5 columns (Zymo Research). DNA
417 free RNA samples were used for rRNA removal by using RiboMinus™ rRNA Removal Kit
418 (Bacteria; Thermo Fisher Scientific) and final purification was performed using the RNA
419 Clean & Concentrator-5 columns (Zymo Research). rRNA depleted samples were used
420 for library preparation using the KAPA mRNA HyperPrep Kits (Roche) by following the
421 manufacturer's instructions. Following the library preparation, the final concentrations of
422 all libraries (Supplementary Table 2) were measured using the Qubit® dsDNA HS Assay
423 Kit (Life Technologies), and the average library size was determined using the Agilent
424 2100 Bioanalyzer (Agilent Technologies). The libraries were then pooled in equimolar

425 ratios of 0.6 nM, and sequenced paired end for 300 cycles using the NovaSeq 6000
426 system (Illumina). Differential expression between the resulting transcriptomes was
427 calculated from pair-wise analysis of trimmed mean of M-values (TMM) normalized read
428 counts (79) including fold change, counts-per-million (CPM), and associated p-values
429 using the R-package, edgeR (80). Differential expression data with p-values ≤ 0.05 were
430 considered statistically significant. Genome and RNA sequencing was conducted by MR
431 DNA (Molecular Research LP). All fold change, CPM, and associated p-values resulting
432 from differential expression experiments as described included as supplementary data
433 files TABLE 1 (*P. putida* survivor compared with *P. putida* control). All raw RNAseq data
434 is publicly available at the NCBI Sequence Read Archive (PRJNA577468).

435 **Antibiotic Susceptibility Assays.**

436 The standard growth curve assay was employed to determine the sensitivity of the
437 unexposed *P. putida* and the survivor phenotype towards kanamycin (50 mg/mL),
438 gentamicin (10 mg/mL), and tetracycline (10 mg/mL) antibiotics. The Lauria Bertani (LB)
439 broth without any supplemented antibiotics was used as a control. The test was
440 performed in a 96-well microtiter plate. In a 96-well plate, each well having 200 µL of LB
441 or LB supplemented with an antibiotic was inoculated with a colony of *P. putida.* Next, the
442 absorbance at OD_{620} was recorded using a plate reader every 30 min for 10 hr to examine
443 the growth dynamics of each phenotype. The test was performed in 12 replicates per
444 condition for both phenotypes. Recorded OD_{620} values were plotted using Prism version
445 7.0d with error bars depicting standard deviation of replicate data.

446 **Carbazole Assays.**

447 The alginate was isolated according to Jones *et al*. (81). In brief, both *P. putida* phenotype
448 unexposed to the predatory stress and the survivor phenotype were grown overnight in 2
449 ml LB media and adjusted to an OD_{600} of 1.00. Following centrifugation, 1 ml of
450 supernatant was treated with 2% cetyl pyridinium chloride to precipitate the alginate. The
451 precipitated alginate was further collected by centrifugation. It was resuspended in 1 M
452 NaCl and then re-precipitated in cold isopropanol. Precipitated alginate was suspended
453 in 150 μl 0.9% (w/v) saline solution. Following established protocols (43, 44), a 50 μL
454 aliquot of the isolated alginate and a dilution series of standard alginic acid (Sigma) were
455 mixed with 200 μL of a solution of 25 mM sodium tetraborate in sulfuric acid and added
456 in a 96-well plate. Next, the plate was heated for 10 min at 100 °C in an oven. After cooling
457 at room temperature for 15 min, 50 μl of a 0.125% carbazole solution in absolute ethanol
458 was added. Then, the plate was re-heated at 100 °C for 10 min in an oven and cooled
459 down at room temperature for 15 min. Finally, the plate was read in a CLARIOstar
460 microplate reader (BMG Labtech Inc., Cary, NC, USA) at a wavelength of 550 nm.
461 Quantities of alginate per sample (μg/ml) were calculated from the resulting standard
462 curve of purchase alginic acid, and statistical significance was calculated using an
463 unpaired t test with Welch's correction in Prism 7.0d.

464 **Anti-alginate Dot Plots.**

465 Alginate dot blots were generated using methodology from Lorenz *et al.* with slight
466 modifications (45). Alginate was isolated as previously described, suspended in 150 μl
467 0.9% (w/v) saline solution, and 2 μl aliquots were pipetted onto a nitrocellulose
468 membrane. After air-drying for 30 min, Tris buffered saline-Tween 20 (TBST) with 5%
469 bovine serum albumin (BSA) was used for membrane blocking for 1 h. Membrane was

470 then washed 3x for 10 min with TBST and subsequently incubated with the alginate
471 antibody (Sigma, monoclonal, anti-mouse) overnight at 4°C. The following day, the
472 membrane was washed 3x for 10 min with TBST, incubated with IRDye 800CW Goat
473 anti-mouse (Sigma) for 30 min, rinsed 2x with TBST, and imaged on a LI-COR Odyssey.
474 Average relative intensities for imaged blots comparing isolated alginate from predator
475 unexposed *P. putida* with alginate isolated from the survivor phenotype (n=10) are
476 reported with statistical significance was calculated using an unpaired t test with Welch's
477 correction in Prism 7.0d.

478 **Assessment of Extracellular Pyoverdine**

479 Extracellular pyoverdine fluorescence was detected from supernatants following
480 methodologies Imperi *et al.* and Barrientos-Moreno *et al.* (46, 47). Clarified supernatants
481 from overnight cultivation of 200 μl LB cultures of predator unexposed *P. putida* and the
482 survivor phenotype adjusted to an OD_{600} of 0.07 were generated by centrifugation (10,000
483 rpm, 15m). Fluorescence was recorded at 455 nm upon excitation at 400 nm using a
484 CLARIOstar microplate reader (BMG Labtech Inc., Cary, NC, USA). Sterile LB was used
485 as a negative control to assess background fluorescence. Average relative fluorescence
486 for supernatants from predator unexposed *P. putida* and survivor phenotype cultures
487 (n=12) are reported with statistical significance was calculated using an unpaired t test
488 with Welch's correction in Prism 7.0d.

489 **Metabolite Extraction and Analysis.**

490 For metabolomic analysis, the survivor phenotype and predator unexposed *P. putida*
491 were cultivated on VY/2 agar plates as described in the predation assay. VY/2 agar plates
492 with TM buffer were used as a negative control. The plates were incubated at 30°C for 14

493 days. After the incubation period, agar was chopped and extracted with ethyl acetate
494 (EtOAC). The EtOAc extracts were dried in vacuo to produce crude extracts for LC-
495 MS/MS analysis. The crude extracts from each condition were generated in triplicate and
496 analyzed as previously described (82). LC-MS/MS generated data was converted to
497 .mzML files using MS-Convert, and the GNPS platform (48) was utilized as a dereplication
498 tool to look for the library hits within publicly available natural products libraries. For the
499 statistical analysis, using XCMSonline (49), multigroup analysis with HPLC orbitrap
500 default settings was employed. MZmine 2.53 was used to generate extracted ion
501 chromatograms (83-85).

502 **Author Contributions.**

503 SA performed the experiments. DCS supervised the project. SA and DCS conceived the
504 project, designed the experiments, and wrote the manuscript.

505 **Acknowledgements.**

506 The authors appreciate funding and support from the National Institute of Allergy and
507 Infectious Diseases (R15AI137996) and the National Institute of General Medical
508 Sciences of the National Institutes of Health (P20GM130460). The authors appreciate
509 Scot E. Dowd at MR DNA, Molecular Research LP for assistance throughout sequencing
510 services provided, Dr. Sandeep Misra Manager of the Analytical and Biophysical
511 Chemistry Core associated with the Glycoscience Center of Research Excellence
512 (GlyCORE; P20GM130460) for LC-MS/MS analysis, and Dr. Nicole Ashpole for her
513 assistance with anti-alginate dot blot generation and imaging.

514 **References.**

515 1. Albataineh H, Stevens DC. 2018. Marine Myxobacteria: A Few Good Halophiles. Mar Drugs
516 16.

517 2. Findlay BL. 2016. The Chemical Ecology of Predatory Soil Bacteria. ACS Chem Biol 11:1502-
518 10.
519 3. Munoz-Dorado J, Marcos-Torres FJ, Garcia-Bravo E, Moraleda-Munoz A, Perez J. 2016.
520 Myxobacteria: Moving, Killing, Feeding, and Surviving Together. Front Microbiol 7:781.
521 4. Mohr KI. 2018. Diversity of Myxobacteria-We Only See the Tip of the Iceberg.
522 Microorganisms 6.
523 5. Nair RR, Vasse M, Wielgoss S, Sun L, Yu YN, Velicer GJ. 2019. Bacterial predator-prey
524 coevolution accelerates genome evolution and selects on virulence-associated prey
525 defences. Nat Commun 10:4301.
526 6. Perez J, Moraleda-Munoz A, Marcos-Torres FJ, Munoz-Dorado J. 2016. Bacterial
527 predation: 75 years and counting! Environ Microbiol 18:766-79.
528 7. Livingstone PG, Millard AD, Swain MT, Whitworth DE. 2018. Transcriptional changes when
529 Myxococcus xanthus preys on Escherichia coli suggest myxobacterial predators are
530 constitutively toxic but regulate their feeding. Microb Genom 4.
531 8. Ellis BM, Fischer CN, Martin LB, Bachmann BO, McLean JA. 2019. Spatiochemically
532 Profiling Microbial Interactions with Membrane Scaffolded Desorption Electrospray
533 Ionization-Ion Mobility-Imaging Mass Spectrometry and Unsupervised Segmentation.
534 Anal Chem 91:13703-13711.
535 9. Muller S, Strack SN, Ryan SE, Shawgo M, Walling A, Harris S, Chambers C, Boddicker J,
536 Kirby JR. 2016. Identification of Functions Affecting Predator-Prey Interactions between
537 Myxococcus xanthus and Bacillus subtilis. J Bacteriol 198:3335-3344.
538 10. Xiao Y, Wei X, Ebright R, Wall D. 2011. Antibiotic production by myxobacteria plays a role
539 in predation. J Bacteriol 193:4626-33.
540 11. Sutton D, Livingstone PG, Furness E, Swain MT, Whitworth DE. 2019. Genome-Wide
541 Identification of Myxobacterial Predation Genes and Demonstration of Formaldehyde
542 Secretion as a Potentially Predation-Resistant Trait of Pseudomonas aeruginosa. Front
543 Microbiol 10:2650.
544 12. Erken M, Lutz C, McDougald D. 2013. The rise of pathogens: predation as a factor driving
545 the evolution of human pathogens in the environment. Microb Ecol 65:860-8.
546 13. Justice SS, Hunstad DA, Cegelski L, Hultgren SJ. 2008. Morphological plasticity as a
547 bacterial survival strategy. Nat Rev Microbiol 6:162-8.
548 14. Seiler C, van Velzen E, Neu TR, Gaedke U, Berendonk TU, Weitere M. 2017. Grazing
549 resistance of bacterial biofilms: a matter of predators' feeding trait. FEMS Microbiol Ecol
550 93.
551 15. Weitere M, Bergfeld T, Rice SA, Matz C, Kjelleberg S. 2005. Grazing resistance of
552 Pseudomonas aeruginosa biofilms depends on type of protective mechanism,
553 developmental stage and protozoan feeding mode. Environ Microbiol 7:1593-601.
554 16. Sun S, Noorian P, McDougald D. 2018. Dual Role of Mechanisms Involved in Resistance to
555 Predation by Protozoa and Virulence to Humans. Front Microbiol 9:1017.
556 17. DePas WH, Syed AK, Sifuentes M, Lee JS, Warshaw D, Saggar V, Csankovszki G, Boles BR,
557 Chapman MR. 2014. Biofilm formation protects Escherichia coli against killing by
558 Caenorhabditis elegans and Myxococcus xanthus. Appl Environ Microbiol 80:7079-87.

559 18. Muller S, Strack SN, Hoefler BC, Straight PD, Kearns DB, Kirby JR. 2014. Bacillaene and
560 sporulation protect Bacillus subtilis from predation by Myxococcus xanthus. Appl Environ
561 Microbiol 80:5603-10.
562 19. Muller S, Strack SN, Ryan SE, Kearns DB, Kirby JR. 2015. Predation by Myxococcus xanthus
563 induces Bacillus subtilis to form spore-filled megastructures. Appl Environ Microbiol
564 81:203-10.
565 20. Wang C, Liu X, Zhang P, Wang Y, Li Z, Li X, Wang R, Shang Z, Yan J, He H, Wang J, Hu W, Li
566 Y. 2019. Bacillus licheniformis escapes from Myxococcus xanthus predation by
567 deactivating myxovirescin A through enzymatic glucosylation. Environ Microbiol 21:4755-
568 4772.
569 21. Contreras-Moreno FJ, Munoz-Dorado J, Garcia-Tomsig NI, Martinez-Navajas G, Perez J,
570 Moraleda-Munoz A. 2020. Copper and Melanin Play a Role in Myxococcus xanthus
571 Predation on Sinorhizobium meliloti. Front Microbiol 11:94.
572 22. Perez J, Jimenez-Zurdo JI, Martinez-Abarca F, Millan V, Shimkets LJ, Munoz-Dorado J.
573 2014. Rhizobial galactoglucan determines the predatory pattern of Myxococcus xanthus
574 and protects Sinorhizobium meliloti from predation. Environ Microbiol 16:2341-50.
575 23. Livingstone PG, Morphew RM, Whitworth DE. 2017. Myxobacteria Are Able to Prey
576 Broadly upon Clinically-Relevant Pathogens, Exhibiting a Prey Range Which Cannot Be
577 Explained by Phylogeny. Front Microbiol 8:1593.
578 24. Seccareccia I, Kost C, Nett M. 2015. Quantitative Analysis of Lysobacter Predation. Appl
579 Environ Microbiol 81:7098-105.
580 25. Akbar S, Dowd SE, Stevens DC. 2017. Draft Genome Sequence of Cystobacter ferrugineus
581 Strain Cbfe23. Genome Announc 5.
582 26. Hassett DJ, Howell ML, Ochsner UA, Vasil ML, Johnson Z, Dean GE. 1997. An operon
583 containing fumC and sodA encoding fumarase C and manganese superoxide dismutase is
584 controlled by the ferric uptake regulator in Pseudomonas aeruginosa: fur mutants
585 produce elevated alginate levels. J Bacteriol 179:1452-9.
586 27. Hassett DJ, Howell ML, Sokol PA, Vasil ML, Dean GE. 1997. Fumarase C activity is elevated
587 in response to iron deprivation and in mucoid, alginate-producing Pseudomonas
588 aeruginosa: cloning and characterization of fumC and purification of native fumC. J
589 Bacteriol 179:1442-51.
590 28. Damron FH, Goldberg JB. 2012. Proteolytic regulation of alginate overproduction in
591 Pseudomonas aeruginosa. Mol Microbiol 84:595-607.
592 29. Deretic V, Martin DW, Schurr MJ, Mudd MH, Hibler NS, Curcic R, Boucher JC. 1993.
593 Conversion to mucoidy in Pseudomonas aeruginosa. Biotechnology (N Y) 11:1133-6.
594 30. Li S, Lou X, Xu Y, Teng X, Liu R, Zhang Q, Wu W, Wang Y, Bartlam M. 2019. Structural basis
595 for the recognition of MucA by MucB and AlgU in Pseudomonas aeruginosa. FEBS J
596 286:4982-4994.
597 31. Martin DW, Schurr MJ, Mudd MH, Deretic V. 1993. Differentiation of Pseudomonas
598 aeruginosa into the alginate-producing form: inactivation of mucB causes conversion to
599 mucoidy. Mol Microbiol 9:497-506.
600 32. Matz C, Bergfeld T, Rice SA, Kjelleberg S. 2004. Microcolonies, quorum sensing and
601 cytotoxicity determine the survival of Pseudomonas aeruginosa biofilms exposed to
602 protozoan grazing. Environ Microbiol 6:218-26.

603 33. Drake EJ, Cao J, Qu J, Shah MB, Straubinger RM, Gulick AM. 2007. The 1.8 A crystal
604 structure of PA2412, an MbtH-like protein from the pyoverdine cluster of Pseudomonas
605 aeruginosa. J Biol Chem 282:20425-34.
606 34. Felnagle EA, Barkei JJ, Park H, Podevels AM, McMahon MD, Drott DW, Thomas MG. 2010.
607 MbtH-like proteins as integral components of bacterial nonribosomal peptide
608 synthetases. Biochemistry 49:8815-7.
609 35. Parker DL, Lee SW, Geszvain K, Davis RE, Gruffaz C, Meyer JM, Torpey JW, Tebo BM. 2014.
610 Pyoverdine synthesis by the Mn(II)-oxidizing bacterium Pseudomonas putida GB-1. Front
611 Microbiol 5:202.
612 36. Ringel MT, Bruser T. 2018. The biosynthesis of pyoverdines. Microb Cell 5:424-437.
613 37. Garneau-Tsodikova S, Labby KJ. 2016. Mechanisms of Resistance to Aminoglycoside
614 Antibiotics: Overview and Perspectives. Medchemcomm 7:11-27.
615 38. Li XZ, Plesiat P, Nikaido H. 2015. The challenge of efflux-mediated antibiotic resistance in
616 Gram-negative bacteria. Clin Microbiol Rev 28:337-418.
617 39. Aeschlimann JR. 2003. The role of multidrug efflux pumps in the antibiotic resistance of
618 Pseudomonas aeruginosa and other gram-negative bacteria. Insights from the Society of
619 Infectious Diseases Pharmacists. Pharmacotherapy 23:916-24.
620 40. Matz C, Deines P, Jurgens K. 2002. Phenotypic variation in Pseudomonas sp. CM10
621 determines microcolony formation and survival under protozoan grazing. FEMS Microbiol
622 Ecol 39:57-65.
623 41. Matz C, Kjelleberg S. 2005. Off the hook--how bacteria survive protozoan grazing. Trends
624 Microbiol 13:302-7.
625 42. Matz C, McDougald D, Moreno AM, Yung PY, Yildiz FH, Kjelleberg S. 2005. Biofilm
626 formation and phenotypic variation enhance predation-driven persistence of Vibrio
627 cholerae. Proc Natl Acad Sci U S A 102:16819-24.
628 43. Al Ahmar R, Kirby BD, Yu HD. 2020. Culture of Small Colony Variant of Pseudomonas
629 aeruginosa and Quantitation of its Alginate. J Vis Exp doi:10.3791/60466.
630 44. Knutson CA, Jeanes A. 1968. A new modification of the carbazole analysis: application to
631 heteropolysaccharides. Anal Biochem 24:470-81.
632 45. Lorenz C, Dougherty TJ, Lory S. 2020. Transcriptional Responses of Pseudomonas
633 aeruginosa to Inhibition of Lipoprotein Transport by a Small Molecule Inhibitor. J Bacteriol
634 202.
635 46. Barrientos-Moreno L, Molina-Henares MA, Pastor-Garcia M, Ramos-Gonzalez MI,
636 Espinosa-Urgel M. 2019. Arginine Biosynthesis Modulates Pyoverdine Production and
637 Release in Pseudomonas putida as Part of the Mechanism of Adaptation to Oxidative
638 Stress. J Bacteriol 201.
639 47. Imperi F, Tiburzi F, Visca P. 2009. Molecular basis of pyoverdine siderophore recycling in
640 Pseudomonas aeruginosa. Proc Natl Acad Sci U S A 106:20440-5.
641 48. Wang M, Carver JJ, Phelan VV, Sanchez LM, Garg N, Peng Y, Nguyen DD, Watrous J,
642 Kapono CA, Luzzatto-Knaan T, Porto C, Bouslimani A, Melnik AV, Meehan MJ, Liu WT,
643 Crusemann M, Boudreau PD, Esquenazi E, Sandoval-Calderon M, Kersten RD, Pace LA,
644 Quinn RA, Duncan KR, Hsu CC, Floros DJ, Gavilan RG, Kleigrewe K, Northen T, Dutton RJ,
645 Parrot D, Carlson EE, Aigle B, Michelsen CF, Jelsbak L, Sohlenkamp C, Pevzner P, Edlund A,
646 McLean J, Piel J, Murphy BT, Gerwick L, Liaw CC, Yang YL, Humpf HU, Maansson M, Keyzers

647 RA, Sims AC, Johnson AR, Sidebottom AM, Sedio BE, et al. 2016. Sharing and community
648 curation of mass spectrometry data with Global Natural Products Social Molecular
649 Networking. Nat Biotechnol 34:828-837.
650 49. Domingo-Almenara X, Montenegro-Burke JR, Ivanisevic J, Thomas A, Sidibe J, Teav T,
651 Guijas C, Aisporna AE, Rinehart D, Hoang L, Nordstrom A, Gomez-Romero M, Whiley L,
652 Lewis MR, Nicholson JK, Benton HP, Siuzdak G. 2018. XCMS-MRM and METLIN-MRM: a
653 cloud library and public resource for targeted analysis of small molecules. Nat Methods
654 15:681-684.
655 50. Dietrich LE, Price-Whelan A, Petersen A, Whiteley M, Newman DK. 2006. The phenazine
656 pyocyanin is a terminal signalling factor in the quorum sensing network of Pseudomonas
657 aeruginosa. Mol Microbiol 61:1308-21.
658 51. Sakhtah H, Koyama L, Zhang Y, Morales DK, Fields BL, Price-Whelan A, Hogan DA, Shepard
659 K, Dietrich LE. 2016. The Pseudomonas aeruginosa efflux pump MexGHI-OpmD transports
660 a natural phenazine that controls gene expression and biofilm development. Proc Natl
661 Acad Sci U S A 113:E3538-47.
662 52. Schiessl KT, Hu F, Jo J, Nazia SZ, Wang B, Price-Whelan A, Min W, Dietrich LEP. 2019.
663 Phenazine production promotes antibiotic tolerance and metabolic heterogeneity in
664 Pseudomonas aeruginosa biofilms. Nat Commun 10:762.
665 53. Sporer AJ, Beierschmitt C, Bendebury A, Zink KE, Price-Whelan A, Buzzeo MC, Sanchez LM,
666 Dietrich LEP. 2018. Pseudomonas aeruginosa PumA acts on an endogenous phenazine to
667 promote self-resistance. Microbiology (Reading) 164:790-800.
668 54. Blankenfeldt W, Kuzin AP, Skarina T, Korniyenko Y, Tong L, Bayer P, Janning P, Thomashow
669 LS, Mavrodi DV. 2004. Structure and function of the phenazine biosynthetic protein PhzF
670 from Pseudomonas fluorescens. Proc Natl Acad Sci U S A 101:16431-6.
671 55. Blankenfeldt W, Parsons JF. 2014. The structural biology of phenazine biosynthesis. Curr
672 Opin Struct Biol 29:26-33.
673 56. Mavrodi DV, Peever TL, Mavrodi OV, Parejko JA, Raaijmakers JM, Lemanceau P, Mazurier
674 S, Heide L, Blankenfeldt W, Weller DM, Thomashow LS. 2010. Diversity and evolution of
675 the phenazine biosynthesis pathway. Appl Environ Microbiol 76:866-79.
676 57. Parsons JF, Song F, Parsons L, Calabrese K, Eisenstein E, Ladner JE. 2004. Structure and
677 function of the phenazine biosynthesis protein PhzF from Pseudomonas fluorescens 2-79.
678 Biochemistry 43:12427-35.
679 58. Bull CT, Shetty KG, Subbarao KV. 2002. Interactions Between Myxobacteria, Plant
680 Pathogenic Fungi, and Biocontrol Agents. Plant Dis 86:889-896.
681 59. Leong W, Lutz, C., Williams, J., Yan, H.P., Benny, Y.K.Y., Chua, C., Rice, S.A., Givskov, M.,
682 Sanderson-Smith, M., McDougald, D. 2020. *Pseudomonas aeruginosa* isolates co-
683 incubated with *Acanthamoeba castellanii* exhibit phenotypes similar to chronic cystic
684 fibrosis isolates. *bioRxiv* doi:https://doi.org/10.1101/2020.02.25.964320.
685 60. Winstanley C, O'Brien S, Brockhurst MA. 2016. Pseudomonas aeruginosa Evolutionary
686 Adaptation and Diversification in Cystic Fibrosis Chronic Lung Infections. Trends Microbiol
687 24:327-337.
688 61. Malone JG. 2015. Role of small colony variants in persistence of Pseudomonas aeruginosa
689 infections in cystic fibrosis lungs. Infect Drug Resist 8:237-47.

690 62. Maunders E, Welch M. 2017. Matrix exopolysaccharides; the sticky side of biofilm
691 formation. FEMS Microbiol Lett 364.
692 63. Sun S, Kjelleberg S, McDougald D. 2013. Relative contributions of Vibrio polysaccharide
693 and quorum sensing to the resistance of Vibrio cholerae to predation by heterotrophic
694 protists. PLoS One 8:e56338.
695 64. Butt AT, Thomas MS. 2017. Iron Acquisition Mechanisms and Their Role in the Virulence
696 of Burkholderia Species. Front Cell Infect Microbiol 7:460.
697 65. Chekabab SM, Daigle F, Charette SJ, Dozois CM, Harel J. 2013. Shiga toxins decrease
698 enterohaemorrhagic Escherichia coli survival within Acanthamoeba castellanii. FEMS
699 Microbiol Lett 344:86-93.
700 66. Lainhart W, Stolfa G, Koudelka GB. 2009. Shiga toxin as a bacterial defense against a
701 eukaryotic predator, Tetrahymena thermophila. J Bacteriol 191:5116-22.
702 67. Steinberg KM, Levin BR. 2007. Grazing protozoa and the evolution of the Escherichia coli
703 O157:H7 Shiga toxin-encoding prophage. Proc Biol Sci 274:1921-9.
704 68. Matz C, Moreno AM, Alhede M, Manefield M, Hauser AR, Givskov M, Kjelleberg S. 2008.
705 Pseudomonas aeruginosa uses type III secretion system to kill biofilm-associated
706 amoebae. ISME J 2:843-52.
707 69. Riquelme S, Varas M, Valenzuela C, Velozo P, Chahin N, Aguilera P, Sabag A, Labra B,
708 Alvarez SA, Chavez FP, Santiviago CA. 2016. Relevant Genes Linked to Virulence Are
709 Required for Salmonella Typhimurium to Survive Intracellularly in the Social Amoeba
710 Dictyostelium discoideum. Front Microbiol 7:1305.
711 70. Pombinho R, Camejo A, Vieira A, Reis O, Carvalho F, Almeida MT, Pinheiro JC, Sousa S,
712 Cabanes D. 2017. Listeria monocytogenes CadC Regulates Cadmium Efflux and Fine-tunes
713 Lipoprotein Localization to Escape the Host Immune Response and Promote Infection. J
714 Infect Dis 215:1468-1479.
715 71. Vieira A, Ramesh A, Seddon AM, Karlyshev AV. 2017. CmeABC Multidrug Efflux Pump
716 Contributes to Antibiotic Resistance and Promotes Campylobacter jejuni Survival and
717 Multiplication in Acanthamoeba polyphaga. Appl Environ Microbiol 83.
718 72. Perez J, Munoz-Dorado J, Brana AF, Shimkets LJ, Sevillano L, Santamaria RI. 2011.
719 Myxococcus xanthus induces actinorhodin overproduction and aerial mycelium
720 formation by Streptomyces coelicolor. Microb Biotechnol 4:175-83.
721 73. Miskinyte M, Sousa A, Ramiro RS, de Sousa JA, Kotlinowski J, Caramalho I, Magalhaes S,
722 Soares MP, Gordo I. 2013. The genetic basis of Escherichia coli pathoadaptation to
723 macrophages. PLoS Pathog 9:e1003802.
724 74. Scanlan PD, Buckling A. 2012. Co-evolution with lytic phage selects for the mucoid
725 phenotype of Pseudomonas fluorescens SBW25. ISME J 6:1148-58.
726 75. Yang F, Gu J, Zou J, Lei L, Jing H, Zhang J, Zeng H, Zou Q, Lv F, Zhang J. 2018. PA0833 Is an
727 OmpA C-Like Protein That Confers Protection Against Pseudomonas aeruginosa Infection.
728 Front Microbiol 9:1062.
729 76. Mulcahy LR, Burns JL, Lory S, Lewis K. 2010. Emergence of Pseudomonas aeruginosa
730 strains producing high levels of persister cells in patients with cystic fibrosis. J Bacteriol
731 192:6191-9.

732 77. Jeanson S, Floury J, Gagnaire V, Lortal S, Thierry A. 2015. Bacterial Colonies in Solid Media
733 and Foods: A Review on Their Growth and Interactions with the Micro-Environment. Front
734 Microbiol 6:1284.
735 78. Reyrolle J, Letellier F. 1979. Autoradiographic study of the localization and evolution of
736 growth zones in bacterial colonies. J Gen Microbiol 111:399-406.
737 79. Dillies MA, Rau A, Aubert J, Hennequet-Antier C, Jeanmougin M, Servant N, Keime C,
738 Marot G, Castel D, Estelle J, Guernec G, Jagla B, Jouneau L, Laloe D, Le Gall C, Schaeffer B,
739 Le Crom S, Guedj M, Jaffrezic F, French StatOmique C. 2013. A comprehensive evaluation
740 of normalization methods for Illumina high-throughput RNA sequencing data analysis.
741 Brief Bioinform 14:671-83.
742 80. Robinson MD, McCarthy DJ, Smyth GK. 2010. edgeR: a Bioconductor package for
743 differential expression analysis of digital gene expression data. Bioinformatics 26:139-40.
744 81. Jones CJ, Ryder CR, Mann EE, Wozniak DJ. 2013. AmrZ modulates Pseudomonas
745 aeruginosa biofilm architecture by directly repressing transcription of the psl operon. J
746 Bacteriol 195:1637-44.
747 82. Adaikpoh BI, Akbar S, Albataineh H, Misra SK, Sharp JS, Stevens DC. 2020. Myxobacterial
748 Response to Methyljasmonate Exposure Indicates Contribution to Plant Recruitment of
749 Micropredators. Front Microbiol 11:34.
750 83. Katajamaa M, Miettinen J, Oresic M. 2006. MZmine: toolbox for processing and
751 visualization of mass spectrometry based molecular profile data. Bioinformatics 22:634-
752 6.
753 84. Olivon F, Grelier G, Roussi F, Litaudon M, Touboul D. 2017. MZmine 2 Data-Preprocessing
754 To Enhance Molecular Networking Reliability. Anal Chem 89:7836-7840.
755 85. Pluskal T, Castillo S, Villar-Briones A, Oresic M. 2010. MZmine 2: modular framework for
756 processing, visualizing, and analyzing mass spectrometry-based molecular profile data.
757 BMC Bioinformatics 11:395.
758

759

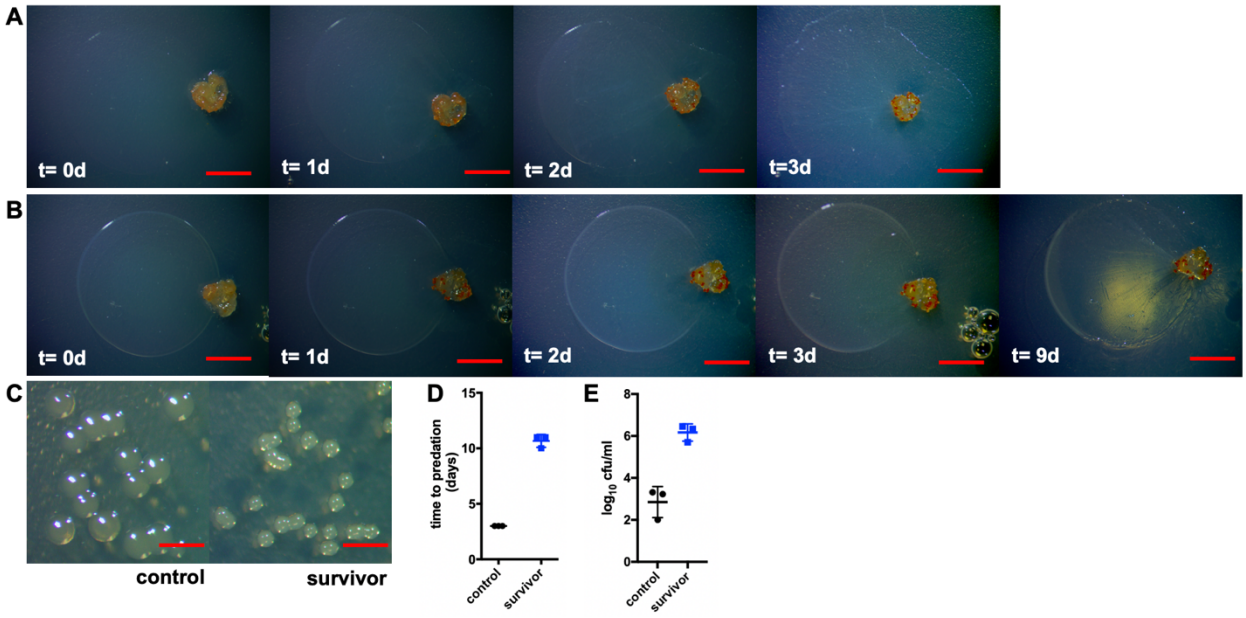

760 **Figure 1:** A) 4 day sequence of *C. ferrugineus* predation of *P. putida* with complete
761 swarming of prey (t= d3). B) 4 day sequence depicting predator avoidance observed from
762 *P. putida* survivor phenotype including an additional image from day 9 to demonstrate
763 length of avoidance. C) Comparison of colony sizes of predator unexposed *P. putida* (left)
764 and *P. putida* survivor phenotype (right) depicting small colony variance of the survivor
765 phenotype. D) Time to predation data for *P. putida* control and *P. putida* survivor
766 phenotype (n=3; $p \leq 0.002$) with E) end point colony forming unit data (n=3; $p \leq 0.006$) to
767 determine differences in cell viabilities post-swarming. Unpaired t-test with Welch's
768 correction used for statistical analyses included in D and E; all scale bars depict 1mm.

769

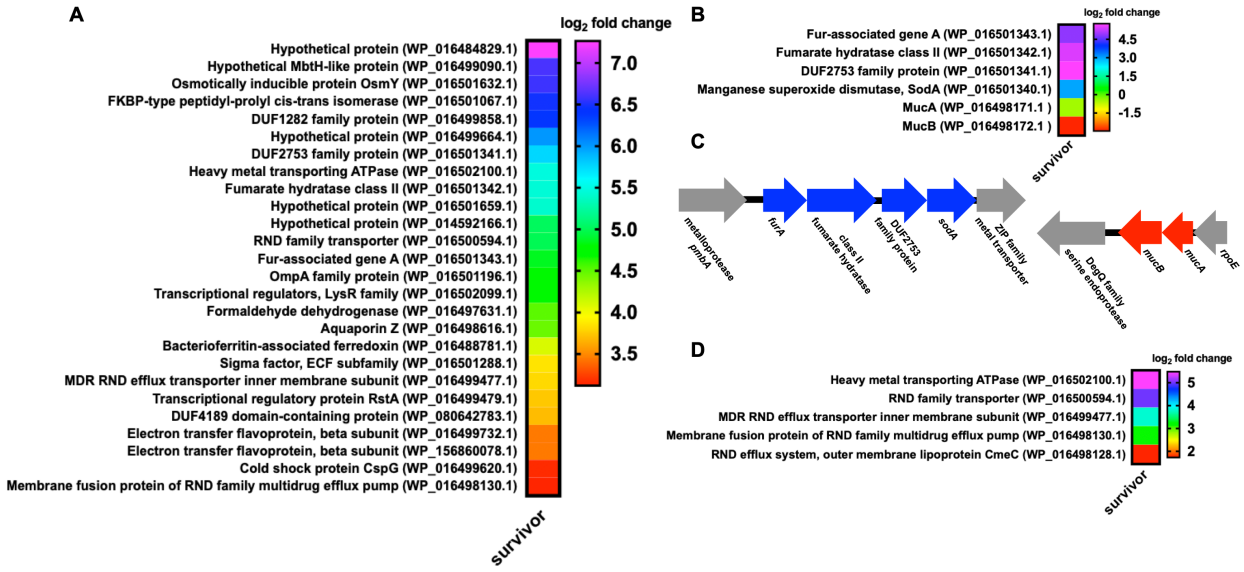

770 **Figure 2:** A) Most abundantly over-expressed genes from survivor phenotype when
771 compared to predator unexposed *P. putida*. B) Up-regulated features associated with
772 alginate production and the associated genomic context for each (C). D) Up-regulated
773 transport proteins including those associated with antibiotic efflux. All data depicted as an
774 averages from 3 biological replicates ($p \leq 0.05$).

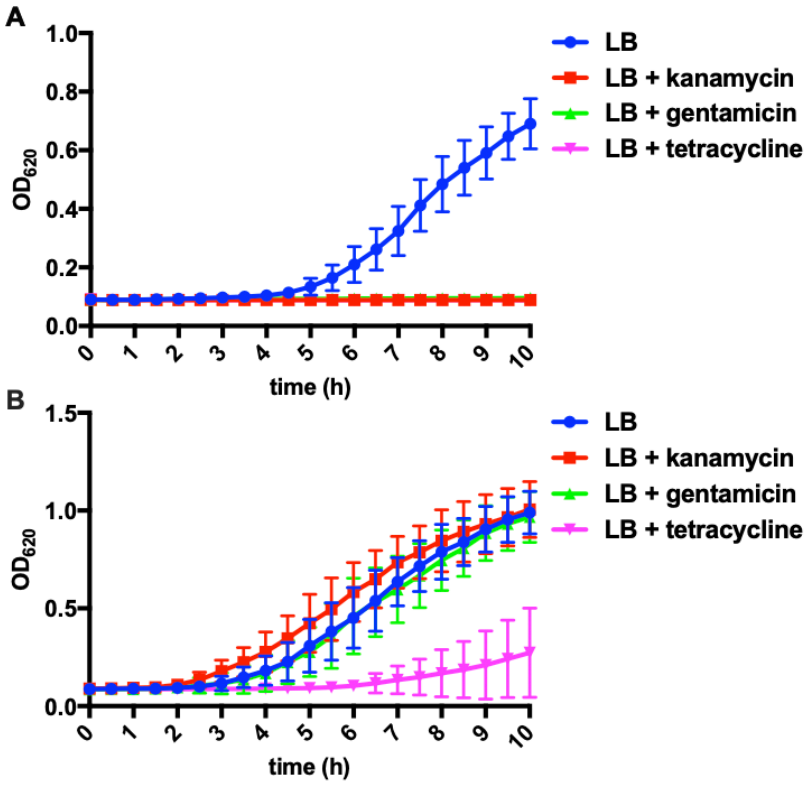

775 **Figure 3:** Growth curves for predator unexposed *P. putida* (A) and *P. putida* survivor
776 phenotype (B) depicting antibiotic resistance unique to the survivor phenotype (n=12). LB
777 supplemented with gentamicin (10 μg/ml), kanamycin (50 μg/ml), and tetracycline (10
778 μg/ml) where indicated.

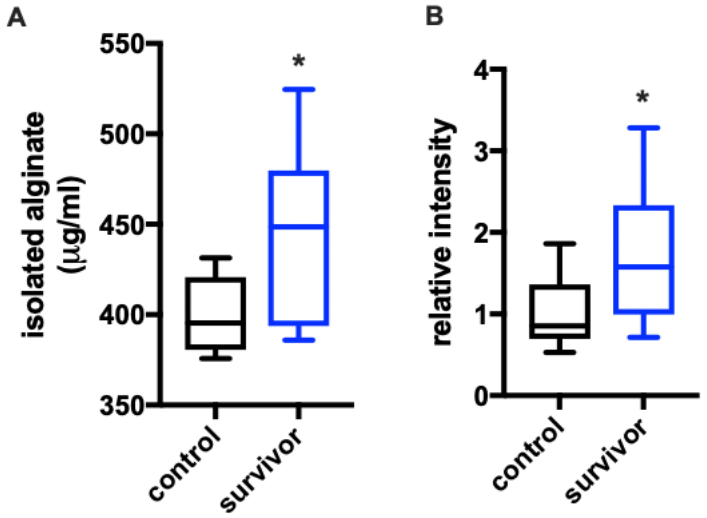

Figure 4: A) Isolated alginate concentration determined from carbazole assays depicting increased alginate production observed from the survivor phenotype (n=16; p≤0.02). B) Relative intensities of alginate dot blots generated from isolated alginate also depicting increased alginate production observed from the survivor phenotype (n=10; p=0.039). Relative units determined from average of control values with statistical significance calculated from an unpaired t test with Welch's correction.

794

795

796

797

798

799

800

801

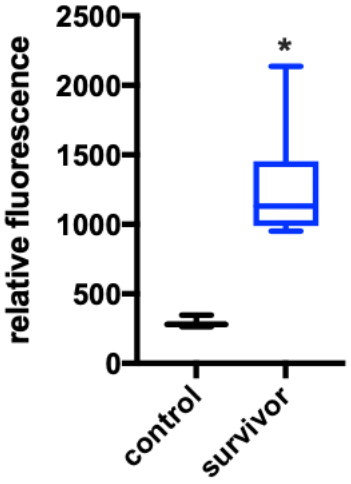

802 **Figure 5:** Relative fluorescence of extracellular pyoverdine depicting increased

803 pyoverdine production from the survivor phenotype (n=12; p≤0.0001). Relative units

804 determined from average of control values with statistical significance calculated from an

805 unpaired t test with Welch's correction.

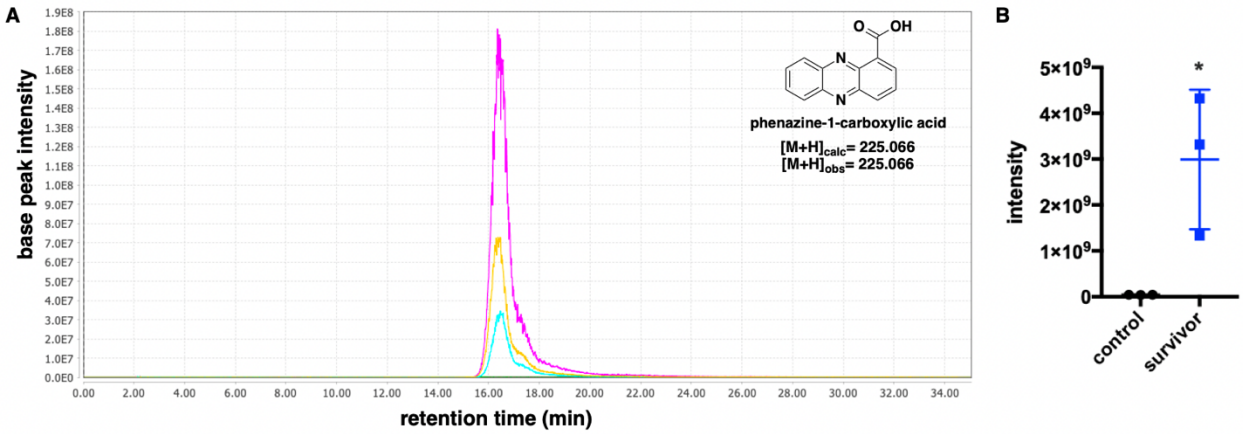

806 **Figure 6:** A) Extracted ion chromatograph (224.9-225.1 m/z) depicting presence of
807 phenazine-1-carboxylic acid in extracts from survivor phenotype replicates (n=3;
808 magenta, yellow, cyan) and absence in extracts from predator unexposed *P. putida*
809 replicates (n=3; red, blue, green). Chromatograph rendered with MZmine v2.37. B)
810 Comparison of detected phenazine-1-carboxylic acid in predator unexposed *P. putida*
811 extracts (labelled control) and survivor phenotype extracts (blue). Box plot data and
812 statistical analysis (n=3; p=0.0509) generated by XCMS v3.7.1 and figure rendered with
813 Prism v7.0d.

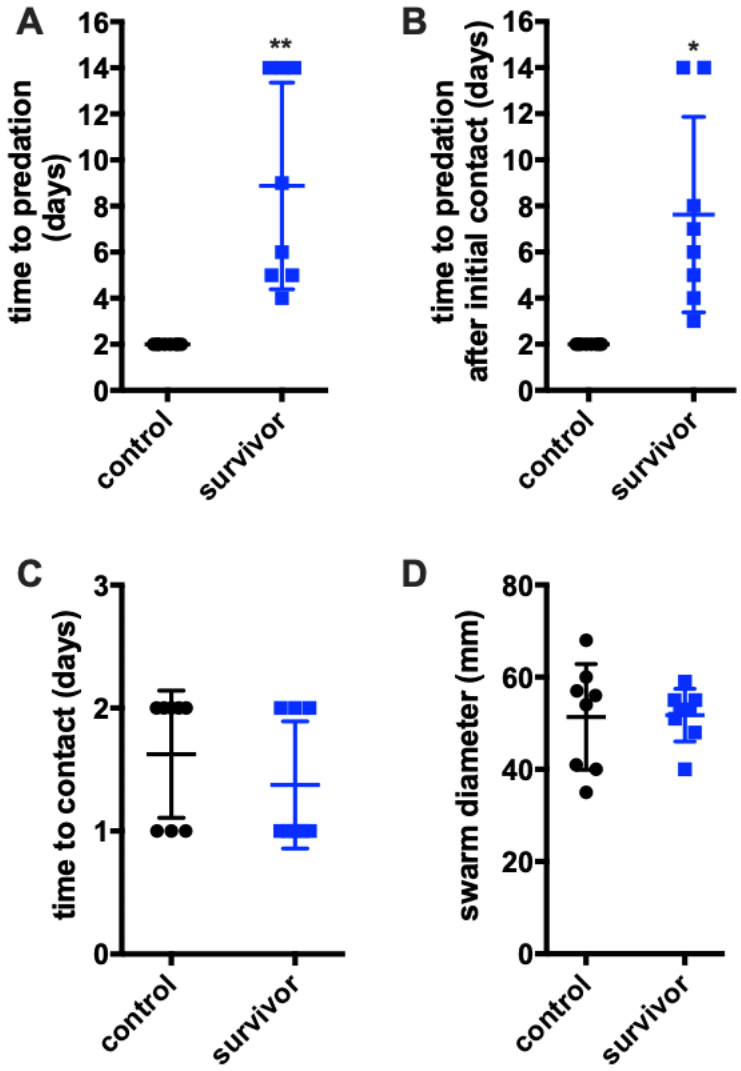

Figure 7: A) Direct contact predation assay as depicted in Figure 1 comparing control (predator unexposed) *P. putida* with freezer stocks of the survivor phenotype (biological replicates) (n=8; p≤0.0001). B) Modified indirect contact predation assay with prey introduced 2 cm from predator (n=8; p≤0.01) and time to predator-prey contact recorded (C). Swarming assays with *C. ferrugineus* plated on prey lawns and swarming diameters recorded after 7 days (n=8). Statistical significance calculated using an unpaired t test with Welch's correction.